Atmos. Chem. Phys. Discuss., 14, 12887–12930, 2014
www.atmos-chem-phys-discuss.net/14/12887/2014/
doi:10.5194/acpd-14-12887-2014

Atmospheric Chemistry and Physics Discussions
Open Access

Particle-area dependence of mineral dust in the immersion mode: investigations with freely suspended drops in an acoustic levitator

K. Diehl[1], **M. Debertshäuser**[1], **O. Eppers**[1], **H. Schmithüsen**[1], **S. K. Mitra**[1], and **S. Borrmann**[2]

[1]Institute of Atmospheric Physics, University of Mainz, Germany
[2]Max Planck Institute for Chemistry, Mainz, Germany

Received: 19 March 2014 – Accepted: 11 April 2014 – Published: 20 May 2014

Correspondence to: K. Diehl (kdiehl@uni-mainz.de)

Published by Copernicus Publications on behalf of the European Geosciences Union.

Abstract

The heterogeneous freezing temperatures of supercooled drops were measured by using an acoustic levitator. This technique allows to freely suspending single drops in air without electrical charges thereby avoiding any electrical influences which may affect the freezing process. Heterogeneous nucleation caused by several mineral dust particles (montmorillonite, two types of illite) was investigated in the immersion mode. Drops of 1 mm in radius were monitored by a video camera during cooling down to −28 °C to simulate the tropospheric temperature range. The surface temperature of the drops was remotely determined with an infra-red thermometer so that the onset of freezing was indicated. For comparisons, measurements with one particle type were additionally performed in the Mainz vertical wind tunnel with drops of 340 µm radius freely suspended. The data were interpreted regarding the particle surfaces immersed in the drops. Immersion freezing was observed in a temperature range between −13 and −26 °C in dependence of particle type and surface area per drop. The results were evaluated by applying two descriptions of heterogeneous freezing, the stochastic and the singular model.

1 Introduction

The types and quantities of atmospheric ice nuclei affect ice cloud microphysical and radiative properties as well as their precipitation efficiency. This has been shown by model studies as, e.g., Phillips et al. (2007), Storelvmo et al. (2008), and Hoose et al. (2008). The role of mineral dust particles as ice nuclei is undoubted (e.g., Hoose and Möhler, 2012). The most abundant minerals occurring in desert aerosols are quartz, calcite, mica, hematite, illite, and gypsum (Kandler et al., 2007). So far, laboratory experiments of heterogeneous freezing have been performed mainly with kaolinite, montmorillonite, and illite (e.g., Hoffer, 1961; Pitter and Pruppacher, 1973; Murray et al., 2011; Pinti et al., 2012; Broadley et al., 2012), and Arizona test dust or several types of natural dust (e.g., Vali, 2008; Connolly et al., 2009; Niedermeier et al., 2011).

To investigate drop freezing in the immersion mode various experimental techniques are available; see the review paper of Hoose and Möhler (2012). These are, for instance, drop freezing devices with cooled surfaces (e.g., Zuberi et al., 2002; Knopf et al., 2011), emulsified drop freezing (e.g., Hoffer, 1961; Pummer et al., 2012), flow tubes (e.g., Niedermeier et al., 2011), continuous flow diffusion chambers (e.g., DeMott et al., 1999; Lüönd et al., 2010), cloud chambers (e.g., Connolly et al., 2009; Niemand et al., 2012), falling droplet chambers (Ladino et al., 2011), acoustic drop levitators (e.g., Ettner et al., 2004; Diehl et al., 2009), vertical wind tunnels (e.g., Pitter and Pruppacher, 1973; Diehl et al., 2002), and, for homogeneous freezing, electrodynamical drop levitators (e.g., Duft and Leisner, 2004).

The lack of most of these methods is that the drops are not freely suspended in air at their terminal velocities during freezing except for vertical wind tunnels; contact-free levitation at least is achieved by electrodynamical and acoustic drop levitators. In contrast to electrodynamical drop levitators, the presence of electrical charges on the drops which might affect the freezing process are not required in acoustic drop levitators. The advantage over measurements in a vertical wind tunnel is that the drops can be levitated for long time periods and are very still which allows to directly determine the surface temperature of the drops during the entire freezing process. The majority of the experiments were performed with two types of illite particles, some studies were undertaken with montmorillonite. For comparisons, measurements with one particle type were additionally performed in the Mainz vertical wind tunnel.

2 Experimental details

2.1 Acoustic levitator

The acoustic levitator was also used in two earlier studies of the freezing of supercooled binary and ternary solution drops (Ettner et al., 2004; Diehl et al., 2009). As the freezing of solution drops requires very low ambient temperatures, these experiments were performed by moving the acoustic trap down into a deep freezer with temperatures reaching as low as −85 °C. During the present experiments, the acoustic levitator was installed inside a walk-in cold chamber which achieves ambient temperatures down to −35 °C. These are sufficient for heterogeneous freezing of water drops. As an improvement to the earlier experiments, an infra-red thermometer was used to determine the drop surface temperature.

2.1.1 Instruments and data acquisition

The employed acoustic levitator is the type APOS BA 10 from the company TEC5 as shown in Fig. 1. Inside the trap an ultrasonic wave is produced by a piezoelectric oscillator and reflected by a concave Teflon reflector plate. The interference generates a standing wave with five nodes between the radiator and the reflector. While the source is fixed the reflector is movable mounted on a micrometer screw. In this way the distance between the source and the reflector can be varied by several millimetres to achieve optimal reflector separation at the operating frequency and temperature. Also, optimally, at the third of the five existing nodes drops with diameters between 100 µm and 3 mm can be levitated. The trap was surrounded by an acrylic glass cylinder to protect the levitated drops from the outside air motions of the walk-in cold chamber in order to establish stable temperature conditions during the experiments. The set-up in the cold chamber (see Fig. 2) includes the acoustic levitator, a platinum-resistor thermometer Pt100, a digital video camera (FireWire-CAM-011H from Phytec), and an infra-red thermometer (KT 19.82 II from Heitronics). The Pt100 sensor was located

ACPD
14, 12887–12930, 2014

in the vicinity of the drop to measure the ambient temperature. The video camera and the infra-red thermometer were mounted on adjustable laboratory stages and arranged around the levitator on sliding rails so that their height and distance to the suspended drop could be adjusted. The video camera allowed a visual observation of the freezing process and size determination of the freezing drops. The infra-red thermometer was used to measure the surface temperature of the freezing drops with an accuracy of 0.7 K. It was calibrated before each series of experiments by use of a Pt100 as reference. For the calibration the Pt100 was coated with a layer of water by dipping it in water which subsequently froze bellow 0 °C. The ice covered temperature sensor represents the drop surface emissivity in a more realistic way.

The advantage of the acoustic levitator is that the drops are held stationary with a positional precision which can not be achieved in wind tunnel experiments. When the ultra-sonic field is kept well isolated from ambient air disturbances, no drop movements are visible with the naked eye. This allows performing direct and contact-free temperature measurements of the drop surface during the entire freezing process. As the area of surface temperature observation is a circular spot of approximately 1 mm in diameter a spherical drop shape is desired but the ultra-sonic field causes an oblate deformation of the drop. This deformation is minimized by lowering the input power to the radiator or by increasing the distance between the radiator and the reflector plate which indirectly reduces the power of the ultra-sonic standing wave field. On the other hand, both adjustments lead to a reduced stability of the floated drop. Thus, these two factors, area of temperature observation and stability of the floated drop, require a compromise between a more stable flattened drop and a less stable spherical drop. Another disturbance is the tendency of the drops to oscillate, in particular directly after inserting the drop into the levitator. By temporarily increasing the distance between the radiator and the reflector plate, the initiated oscillations are restrained.

All measuring instruments were arranged around the acoustic levitator inside the cold chamber. Several windows in the protecting acrylic glass tube allow the observation of the levitated drops: a zinc selenide lens for the infra-red thermometer, an optical filter

ACPD
14, 12887–12930, 2014

for the video camera, a hole for the Pt100 sensor, and, furthermore, a shutter to inject the drops. A Teflon-coated needle from which the drops could be easily released was used to place the drops at the ultrasonic standing wave node.

To control, record, and store the experimental parameters, a PC with the application software LabView was used. The signals of the video camera were monitored on the outside PC so that the drop could be observed on-line during freezing. The transition from the liquid to the ice phase became visible from the change of the transparent liquid drop to an opaque frozen drop as recorded from the video camera but it was clearly defined by the temporal development of the drop surface temperature recorded by the infra-red thermometer.

2.1.2 Experimental procedure

The investigated drops had sizes of 1 mm radius which is larger than cloud drops but is in the range of raindrops (Pruppacher and Klett, 1997). However, as mentioned above, this drop size was required to perform the measurement of the drop surface temperature. Prior to the heterogeneous freezing experiments, the levitator was cleaned by rinsing with purified water and blank checks were performed. Drops generated from pure distilled and de-ionised water of 1 mm radius did not freeze within the experimental time periods of less than a minute at temperatures above −35 °C which is to be expected when no ice nuclei are present (Pruppacher and Klett, 1997).

The measurement of the drop surface temperature allows to clearly determining the onset of freezing. Figure 3 shows an example for the temperature development during freezing. According to Hindmarsh et al. (2003) it can be divided into four stages: 1. supercooling stage before the phase change sets in; here the temperature decreases. 2. Recalescence stage which is characterised by a sudden temperature increase. Latent heat is released when the phase change is initiated so that the surface temperature of the drop reaches almost 0 °C. 3. Freezing stage which is a rather long time period where the entire drop freezes; at the end, the temperature decreases again; 4. Cooling stage after the drop is entirely frozen.

ACPD
14, 12887–12930, 2014

For the freezing experiments the cold chamber was always pre-cooled to a low temperature around $-30 \pm 1\,^{\circ}$C. Thus, the cooling rate of the drops, i.e. the rate by which the drop temperature was adapted to the ambient temperature was the same during all experiments. The development of the drop surface temperature with time was measured several times with pure water drops. The drops reached a lowest temperature of $-27 \pm 0.7\,^{\circ}$C only because the levitator was isolated against the cold chamber air (see Sect. 2.1.1). From the measurements the following equation was derived to describe the drop temperature $T_{\mathrm{drop}}(t)$ in °C:

$$T_{\mathrm{drop}}(t) = -27.050\,^{\circ}\mathrm{C} + 27.082\,^{\circ}\mathrm{C}\exp\left(-\frac{t}{16.374}\right) \quad (1)$$

with the time t in s and the result is shown in Fig. 4. Drops were generated from distilled water which was mixed with the selected mineral dust particles in defined amounts. During the experiments, this solution was continuously stirred to avoid a settling and agglomeration of the particles. It was kept inside the cold chamber at a constant temperature slightly above $0\,^{\circ}$C. Individual drops were levitated one after another until they froze and the freezing temperatures, i.e. the lowest surface temperatures were recorded. For each particle type and concentration, approximately 100 drops were observed.

2.2 Vertical wind tunnel

In the Mainz vertical wind tunnel drops from micrometer to millimetre sizes are freely floated at their terminal velocities in a vertical air stream. Thus, ventilation and heat transfer are similar to the situation as in the real atmosphere. The experiments were performed similar as described in Diehl et al. (2002) and v. Blohn et al. (2005) where immersion freezing of pollen was investigated. Detailed descriptions of the wind tunnel are given therein and in the review paper of Diehl et al. (2011). To perform ice nucleating experiments, the tunnel can be cooled down to $-30\,^{\circ}$C. Air sucked in from outside is passed through particle filters to avoid the presence of possible ice nuclei during the

ACPD
14, 12887–12930, 2014

experiments. This was ensured in the way that it was proven that drops containing no particles did not freeze within the investigated temperature range. For the immersion freezing experiments, the wind tunnel was pre-cooled to certain temperatures in steps of 1 K so that, in contrast to the acoustic trap experiments, drop freezing was observed at constant temperatures. Particles were mixed with distilled water in defined concentrations and drops formed from this mixture were injected into the wind tunnel. For each temperature and particle type, 40 to 50 drops were investigated. The onset of freezing was determined by observation and is characterized by an opaque look of the drops and a different floating behaviour.

As an improvement to earlier measurements, the fractions of frozen drops were determined time-resolved. When a drop started floating, a time recording was started until the drop froze. The total observation time per drop was 30 s, i.e. drops which did not freeze within this time period were counted as unfrozen. Wind speed, temperature, and relative humidity of the tunnel air were recorded continuously. These parameters were required to calculate afterwards the drop sizes and the drop surface temperatures.

As the air velocity in the tunnel must be equal to the terminal velocity of the floated drop to keep it floating in the observation section the drop size could be determined from the recorded wind speed (v. Blohn et al., 2005). In order to obtain similar sized drops for the experiments only those drops were observed which were suspended in a rather narrow wind speed range of $2.70 \pm 0.25\,\mathrm{m\,s^{-1}}$. From this terminal velocity the average drop size was calculated according to Pruppacher and Klett (1997) to $340 \pm 30\,\mu\mathrm{m}$. The drops observed in the wind tunnel were smaller than the ones used in the acoustic trap but still larger than cloud droplets. This was a required compromise as drop freezing was determined by visual observation. According to Pruppacher and Klett (1997, Chapt. 13) the actual drop temperature while suspended in the wind tunnel and the adaptation time, i.e. the time until the drop temperature is equal to the ambient temperature were calculated from the ambient tunnel air temperature and the dew point of the tunnel air. As shown in Fig. 5, it takes between 3 and 5 s until the temperature of a 370 µm drop reaches the ambient temperature. For the present experimental

ACPD
14, 12887–12930, 2014

conditions, an adaptation time of 4 s was assumed. The measurement accuracy of the drop temperature was estimated as ±1 K.

2.3 Particle samples

Several particle samples were used in the experiments. As first test ice nuclei in the acoustic levitator montmorillonite K10 particles were selected which are commercially available and characterised by a specific surface area of 220 $m^2\,g^{-1}$ (Sigma Aldrich). The majority of the experiments were performed with illite particles. Two types of illite were used: illite IMt1 and illite NX. Illite IMt1 is available from the Clay Mineral Society and according to the manufacturer is consists of 85 to 90 % illite and 10 to 15 % quartz. Particle diameters range from less than 0.2 µm to larger than 63 µm with a maximum of the number size distribution at 1.2 µm (Köster, 1996). Its specific surface area was determined as 31.7 $m^2\,g^{-1}$ (Hiranuma and Möhler, 2013). Illite NX was obtained from B + M Nottenkämper as Arginotec® NX and is composed by 86 % illite, 10 % kaolinite, 4 % calcite, and traces of quartz and feldspar. Its number size spectrum shows a maximum at 0.3 µm diameter, particle sizes are varying from 0.03 to 10 µm and the specific surface area is 124.4 $m^2\,g^{-1}$ (Hiranuma and Möhler, 2013). The latter illite type was selected as a test aerosol to be used in the German research group INUIT and is currently investigated by several different techniques (see INUIT website: www.ice-nuclei.de). According to Broadley et al. (2012) illite NX might be used as a proxy for atmospheric dust as its composition is rather close to atmospheric samples of mineral dust.

ACPD
14, 12887–12930, 2014

3 Results and discussion

3.1 Frozen fractions and median freezing temperatures

3.1.1 Results from acoustic levitator experiments

The particles immersed in the drops were evaluated in terms of particle surface area per drop. These were calculated from the particle concentrations in the stock solution and the average drop size. With illite IMt1 and illite NX particles, three different particle concentrations were investigated, with montmorillonite K10 only one particle concentration. Two illite NX particle concentrations were investigated at the vertical wind tunnel also. The cases are listed in Table 1.

The results indicate that immersion freezing is dependant on the particle surface area in the drop. This confirms the findings of other recent studies as, e.g., Murray et al. (2011), Hartmann et al. (2013), and Broadley et al. (2012). In the following Figs. 6 to 8, same colours represent data for similar particle surface areas per drop. Figures 6 and 7 show the fractions of frozen drops as function of temperature for illite IMt1 and illite NX, respectively, as measured in the acoustic levitator. With decreasing particle surface areas in the drops the median freezing temperature decreases, too, but the differences are reduced towards lower particle surface areas, see Table 1. In case of illite IMt1, the median freezing temperature decreased from −18.8 °C to −23.6 °C when the particle surface area per drop was reduced by one order of magnitude; in case of illite NX, T_{50} decreased from −19.7 °C to −23.7 °C by reducing the particle surface area per drop by two orders of magnitude. Differences between the two illite types with comparable particle surface areas are not significant as they are only slightly higher than the measurement accuracies (±0.7 K): the median freezing temperatures of illite IMt1 are −23.6 ± 0.7 °C and −18.8 ± 0.7 °C for particle surface areas of $3.5 \times 10^{-6}\,m^2\,drop^{-1}$ and $7.0 \times 10^{-5}\,m^2\,drop^{-1}$, respectively, for illite NX median freezing temperatures of −22.8 ± 0.7 °C and −19.7 ± 0.7 °C were measured for particle concentrations of $7.1 \times 10^{-6}\,m^2\,drop^{-1}$ and $7.1 \times 10^{-5}\,m^2\,drop^{-1}$, respectively.

ACPD
14, 12887–12930, 2014

Figure 8 demonstrates the freezing behaviour of montmorillonite K10 in comparison to illite. Although it was present in the drops with a particle surface area of 2.5×10^{-4} m^2 drop^{-1}, i.e. one order of magnitude higher than in the highest cases of illite IMt1 and NX (7.0×10^{-5} and 7.1×10^{-5} m^2 drop^{-1}, respectively), its median freezing temperature does not exceed the ones of illite IMt1 and NX (−20.6 °C in comparison to −18.8 °C and −19.7 °C, see Table 1).

3.1.2 Results from wind tunnel experiments

Figure 9 gives the fractions of frozen drops as function of temperature for illite NX as measured in the wind tunnel for comparable particle surface areas in the drops (represented by same colours as before in Fig. 7). The figure shows accumulated data for the total observation time of 30 s. The median freezing temperatures were −20.8 ± 1 °C and −19.2 ± 1 °C for particle surface areas of 5.1×10^{-6} m^2 drop^{-1} and 5.1×10^{-5} m^2 drop^{-1}, respectively. Thus, the deviations between the results from the two techniques are within the measurement accuracies (see Table 1). As the experiments at the wind tunnel were performed at constant temperatures, the time-resolved freezing fractions are shown in Figs. 10 and 11 for the two investigated particle surface areas. The results indicate that even after an adaptation time of 4 s (marked as black vertical line in the figures) the frozen fraction still increases. At a given temperature, e.g., −21 °C freezing proceeds more slowly with the lower particle surface area 5.1×10^{-6} m^2 per drop (see blue symbols in Figs. 10 and 11). So it is obvious that at lower temperatures and with higher particle surface areas per drop freezing proceeds faster. Such behaviour has been observed also by Murray et al. (2011) and Broadley et al. (2012) in isothermal experiments.

3.1.3 Comparison to literature data

The immersion freezing behaviour of illite NX was investigated by Broadley et al. (2012) for particle surface areas between 1×10^{-11} m^2 to 3×10^{-8} m^2 corresponding to drops with radii between 5 and 40 µm. Thus, in their experiments the drop volumes were at least 4 orders of magnitudes smaller and so were the particle surface areas. In Fig. 12 the median freezing temperatures as determined by Broadley et al. (2012) and the present results (from acoustic levitator and wind tunnel) are shown in green and blue, respectively. Broadley et al. (2012) found an approximately linear increase of the median freezing temperature with the log of the particle surface area per drop for particle surface areas smaller than $6 \times 10^{-10}\,\mathrm{m}^2$ (solid green line in Fig. 12). Afterwards, as indicated by the dotted green line, for small drops T_{50} stays nearly constant but it further increases for larger drops containing a larger particle surface area. This tendency is obvious for the present cases with significantly larger drops and larger particle surface areas: the median freezing approximately increases with the log of the particle surface area. An extrapolation of the regression line (blue solid line in Fig. 12) towards smaller particle surface areas (blue dotted line) comes into the region of the Broadley et al. (2012) results.

3.2 Application of heterogeneous freezing models

Two models were applied to describe heterogeneous freezing, the time-dependant stochastic model and the singular model which neglects time dependence in comparison to particle variability. An important advantage of the singular model is that it allows simplifying the description of ice formation in cloud models (Vali, 2008).

3.2.1 Stochastic model

The stochastic model is initiated by the description of homogeneous freezing where it is assumed that small clusters randomly form in the supercooled liquid phase, only some of them growing further to macroscopic crystals (e.g., Pruppacher and Klett, 1997; Murray et al., 2010). In case that a solid surface is present this stabilizes the clusters of the ice phase. To extend the homogeneous stochastic model to heterogeneous ice nucleation by a single species it is assumed that the nucleating probability is similar for all drops of a population. Thus, the number of drops Δn_{fr} freezing heterogeneously in a time period Δt is given by (Murray et al., 2011):

$$\Delta n_{fr} = N_{total}(1 - \exp(-J(T)\, s\, \Delta t)) \quad (2)$$

with N_{total} the total number of observed drops, s the particle surface area immersed in the drops, and $J(T)$ the nucleation rate coefficient per unit particle surface area and time. With f_{ice} meaning the fraction of frozen drops

$$f_{ice} = \frac{n_{fr}}{N_{total}} \quad (3)$$

as determined in the experiments, and the freezing time t, the nucleation rate coefficients $J(T)$ per unit particle surface area and time can be calculated according to Murray et al. (2011):

$$J(T) = -\frac{\ln(1 - f_{ice})}{s\, t} \quad (4)$$

As Eq. (4) is valid for constant temperatures it is applicable to the wind tunnel experiments only. Following Koop et al. (1997) the freezing time t can be interpreted as the total cumulative observation time, i.e. 30 s as due to the stochastic model each freezing event is independent on the number of previous trials and the different freezing events are not dependant on each other. Figure 13 shows the nucleation rate coefficients $J(T)$ for illite NX present with $5.1 \times 10^{-6}\,m^2$ per drop and $5.1 \times 10^{-5}\,m^2$ per drop derived from the wind tunnel experiments by using Eq. (4). For the limited ranges of particle surface area and temperature the nucleation rate coefficients can be described by a single line within the experimental errors (black line in Fig. 13) thus indicating that the log of the nucleation rate coefficient increases with temperature.

To look closer to the time dependence of freezing, the liquid ratio, i.e. the fractions of drops which remain liquid were calculated as function of time. From Eq. (2) it can be

ACPD
14, 12887–12930, 2014

derived that

$$\ln \frac{n_{\text{liq}}}{N_{\text{total}}} = -J(T)\,s\,t \tag{5}$$

and the results are given in Figs. 14 and 15 for $5.1 \times 10^{-6}\,\text{m}^2$ per drop and $5.1 \times 10^{-5}\,\text{m}^2$ per drop, respectively, for different temperatures. Cases where freezing took place during the cooling stage of the drops were not considered, that means freezing events during the first 4 s (i.e. on the left-hand-side of the vertical line in the figures). One can note that except for one case (at $-21\,^{\circ}$C with $s = 5.1 \times 10^{-6}\,\text{m}^2$ per drop) the data very well follow straight lines indicating the exponential decay of the liquid drops with time at constant temperatures as predicted by Eq. (5). This confirms that nucleation events during the wind tunnel experiments were stochastic processes affected by a single nucleation site type.

To apply the stochastic model to the data measured with the acoustic trap one has to consider the effect of the non-linear cooling rate. For that purpose Eq. (4) was modified as follows. It was assumed that during temperature changes of 1 K the cooling rate was nearly constant. For each temperature in steps of 1 K the total cooling time t was calculated according to Eq. (1). Afterwards, for each temperature change ΔT the required time Δt was calculated and the cooling rate $\gamma(T)$ was determined from

$$\gamma(T) = \frac{\Delta T}{\Delta t} \tag{6}$$

with $\Delta T = 1\,\text{K}$. Thus, for a temperature change from T_1 to T_2 there is a cooling rate according to Eq. (6) and the change of the frozen fraction is given by

$$\Delta\left(\frac{n_f}{N_{\text{total}}}\right) = \frac{\Delta n_f}{N_{\text{total}}} = \frac{n_{f,2}}{N_{\text{total}}} - \frac{n_{f,1}}{N_{\text{total}}} \tag{7}$$

ACPD
14, 12887–12930, 2014

considering that N_{total} is constant. Analogue to Eq. (2), the number of drops Δn_{fr} freezing heterogeneously during a temperature change ΔT is given by

$$\Delta n_f = N_{total} \left(1 - \exp\left(-J(T)\, s\, \Delta T \frac{1}{\gamma(T)}\right)\right) \quad (8)$$

with the cooling rate γ in units of [$\mathrm{K\,s^{-1}}$] and the nucleation rate coefficient $J(T)$ in units of [$\mathrm{area^{-1}\,s^{-1}}$]. Thus, $J(T)$ can be calculated by

$$J(T) = -\frac{\ln\left(1 - \Delta \frac{n_n}{N_{total}}\right)}{s\, \Delta T\, \frac{1}{\gamma(T)}} \quad (9)$$

with $\Delta T = 1\,\mathrm{K}$.

A comparison of the nucleation rate coefficients derived from acoustic levitator and wind tunnel measurements is given in Fig. 16. Results from wind tunnel experiments (derived according to Eq. 4) are shown with their regression line (solid line in black) as in Fig. 13. The dotted black line gives the extrapolation of the regression line towards higher and lower temperatures. Results from acoustic trap experiments were calculated by using the modified Eq. (9). They show a rather large scatter around the regression line; however, in the temperature range below −17 °C they follow the same trend. At higher temperatures the data are located definitely above the extrapolated regression line. This indicates that in the acoustic levitator experiments the freezing rate of the drops during the first 15 s of cooling is overestimated because of the very fast cooling rate in the beginning.

3.2.2 Singular model

Besides the stochastic model, it is suggested that heterogeneous freezing is dominated by the nucleating characteristics of ice-active sites and, thus, only dependant on temperature while the time-dependence, i.e. the stochastic nature of the freezing

ACPD
14, 12887–12930, 2014

process becomes negligible (Vali, 2008). The singular model is based on the assumption that critical clusters form on ice-active sites at characteristic temperatures so that freezing takes place as soon as the characteristic temperature is reached without any time dependence. Thus, if the temperature is held constant one would not observe further freezing events. However, this is not consistent with the present wind tunnel observations and previous measurements (e.g., Murray et al., 2011; Broadley et al., 2012).

According to the singular model of heterogeneous freezing the surface density of active sites $n_s(T)$ per unit particle surface area was determined from the present data as follows (Murray et al., 2011):

$$n_s(T) = -\frac{\ln(1 - f_{ice})}{s} \quad (10)$$

Figure 17 shows the surface densities of active sites n_s for illite NX from both techniques, marked by different colours, for all investigated particle surface areas per drop. The two data sets show a very good agreement within the measurement errors and are represented by one third order polynomial regression curve (solid black line). The data measured with illite IMt1 (Fig. 18) follow a somewhat different trend so that they are represented by another third order polynomial regression curve. A comparison of these regression curves as shown in Fig. 19 (blue and black symbols and lines) indicates that they cross each other at a temperature of −19 °C. The deviations in the other temperature ranges are in most cases slightly outside the measurement errors. In contrast, the results from montmorillonite K10, additionally shown in Fig. 19 in red, lie below the curves for illite and follow another trend. Although data are available only for a limited temperature range this trend indicates a reduced surface density of active sites of montmorillonite which is to be expected according to the results of Atkinson et al. (2013). In general, Figs. 17 to 19 indicate that the lower the temperature the more active sites are available on the ice nucleating material.

ACPD
14, 12887–12930, 2014

3.2.3 Comparison to literature data

The nucleation rate coefficients and surface densities of active sites are compared to the results of Broadley et al. (2012) for immersion freezing of illite NX. In Fig. 20, the area of the Broadley et al. (2012) nucleation rate coefficients for various cooling rates and different particle surface areas between $1 \times 10^{-11}\,m^2$ to $3 \times 10^{-8}\,m^2$ is marked as a grey shaded area. The present results are shown as blue and red symbols (results from acoustic levitator and wind tunnel, respectively). Because of higher particle surface areas they are located in a completely different temperature range but the trend towards lower temperatures shows that they approximate the Broadley et al. (2012) results. In Fig. 21 the surface densities of active sites for illite NX from the present experiments (shown as blue and red symbols, polynomial regression curve from the data as solid line) are compared to the results from Broadley et al. (2012) (green solid line as fit to the data, from Broadley et al., 2012). Although there is a gap between the two lines at a temperature of −25 °C their extrapolations would meet each other.

These comparisons indicate that the present results very well complement the results from Broadley et al. (2012) as the trends observed for lower particle surface areas are confirmed by the present results in the higher temperature range.

4 Summary and conclusions

Immersion freezing was found to occur in a temperature range between −14 and −26 °C in dependence of particle type and mass concentration per drop. The rather high freezing temperatures are due to the drop sizes of 340 µm and 1 mm in radius and, thus, large mass concentrations and particle surface areas per drop. The data were evaluated in terms of nucleation rate coefficients and surface densities of active sites according to both the stochastic and singular models of heterogeneous freezing. The present results very well complement earlier results from Broadley et al. (2012) for illite NX as they investigated smaller drops containing less particle surface areas and

ACPD
14, 12887–12930, 2014

freezing in a lower temperature range. The other type of illite IMt1 used in the present experiments led to similar results although its composition is somewhat different. The findings for montmorillonite K10 indicate a trend towards a lower surface density of ice-active sites as suggested by Atkinson et al. (2013).

The two techniques used in the present investigations both allow freely suspending single drops without electrical charges and wall or substrate contacts but having the disadvantage that the drop sizes are larger than typical cloud drops. In the wind tunnel, the drops reach equilibrium with the ambient temperature within 3 to 5 s and, afterwards, can be kept at a constant temperature during observation. Thus, the time dependence of the freezing process is clearly indicated. In the acoustic levitator, it is not possible to cool down the drops within seconds because of the larger drop volume and the missing ventilated heat transfer. Therefore, they cool down more slowly exchanging heat with the ambient air in the cold chamber which, because of the large drop volume, results in a non-linear cooling rate. The freezing time is coupled to the freezing temperature and cannot be used to determine nucleation rate coefficients.

Because of the constant temperatures during wind tunnel experiments, the stochastic model was applied to those results with the use of the total observation time as freezing time. For the measurements in the acoustic trap, a modification was required to account for the non-linear cooling rate of the drops. This was undertaken by using piecewise linear cooling rates. The resulted nucleation rate coefficients agree well with the ones derived from wind tunnel experiments for temperatures lower than −17 °C.

Although the singular model which neglects time dependence of nucleation does not account for the observations that freezing proceeds with time at constant temperatures, its application to the present wind tunnel and acoustic trap results show a good agreement between the two experimental techniques. The derived number densities of active sites can be used in cloud models to easily describe ice formation in the immersion mode. However, parameterizations applicable in cloud models are not given in the present article as this would be presented in a forthcoming paper. The special mineral dust type illite NX is currently being investigated by a number of different experimental techniques within the frame work of INUIT. A compilation of all results from the entire INUIT community with a general parameterization applicable to model simulations will be presented in a future joint publication.

In spite of some deficiencies the use of the acoustic levitator has a number of essential advantages. It is a small transportable instrument and can be easily installed. It does not require a huge amount of air flow and, thus, energy to establish drop floating and is, therefore, much more economical in its operation. Although in the present experiments the levitator was placed inside a walk-in cold chamber, it might as well be placed inside a table top cold box. The possibility to directly measure the drop temperature with an infra-red thermometer allows to clearly defining the onset of freezing. In particular for nucleation processes, flow hydrodynamics and ventilated heat transfer as it happens in the wind tunnel are not deciding factors as much as the temperature and the cooling rate. If required, a small design modification could bring additional ventilated heat transfer. Thus, the acoustic levitator presents a good alternative to other methods to investigate drop freezing in the immersion mode.

Acknowledgements. This work is part of the research group INUIT (Ice Nuclei research UnIT) and was supported by the Deutsche Forschungsgemeinschaft under grant DI 1539/1-1. We would like to acknowledge the expertise of T. Kisely (Karlsruhe Institute of Technology, Institute for Nuclear Waste Disposal) for the BET measurements of the used illite particle samples.

References

Connolly, P. J., Möhler, O., Field, P. R., Saathoff, H., Burgess, R., Choularton, T., and Gallagher, M.: Studies of heterogeneous freezing by three different desert dust samples, Atmos. Chem. Phys., 9, 2805–2824, doi:10.5194/acp-9-2805-2009, 2009.

DeMott, P. J., Chen, Y., Kreidenweis, S. M., Rogers, D. C., and Sherman, D. E.: Ice formation by black carbon particles, Geophys. Res. Lett., 26, 2429–2432, 1999.

Diehl, K., Matthias-Maser, S., Mitra, S. K., and Jaenicke, R.: The ice nucleating ability of pollen, Part II: Laboratory studies in immersion and contact freezing modes, Atmos. Res., 61, 125–133, 2002.

Diehl, K., Simmel, M., and Wurzler, S.: Numerical simulations of the impact of aerosol properties and drop freezing modes on the glaciation, microphysics, and dynamics of clouds, J. Geophys. Res., 111, D07202, doi:10.1029/2005JD005884, 2006.

Diehl, K., Ettner-Mahl, M., Hannemann, A., and Mitra, S. K.: Homogeneous freezing of single sulfuric and nitric acid solution drops levitated in an acoustic trap, Atmos. Res., 94, 356–361, doi:10.1016/j.atmosres.2009.06.001, 2009.

Diehl, K., Mitra, S. K., Szakáll, M., v. Blohn, N., Borrmann, S., and Pruppacher, H. R.: The Mainz vertical wind tunnel facility: a review of 25 years of laboratory experiments on cloud physics and chemistry, in: Wind Tunnels: Aerodynamics, Models, and Experiments, edited by: Pereira, J. D., Nova Science Publishers Inc., Hauppauge, NY, Chapter 2, 2011.

Duft, D. and Leisner, T.: Laboratory evidence for volume-dominated nucleation of ice in supercooled water microdroplets, Atmos. Chem. Phys., 4, 1997–2000, doi:10.5194/acp-4-1997-2004, 2004.

Ettner, M., Mitra, S. K., and Borrmann, S.: Heterogeneous freezing of single sulfuric acid solution droplets: laboratory experiments utilizing an acoustic levitator, Atmos. Chem. Phys., 4, 1925–1932, doi:10.5194/acp-4-1925-2004, 2004.

Hartmann, S., Augustin, S., Clauss, T., Wex, H., Šantl-Temkiv, T., Voigtländer, J., Niedermeier, D., and Stratmann, F.: Immersion freezing of ice nucleation active protein complexes, Atmos. Chem. Phys., 13, 5751–5766, doi:10.5194/acp-13-5751-2013, 2013.

Hindmarsh, J. P., Russell, A. B., and Chen, X. D.: Experimental and numerical analysis of the temperature transition of a suspended freezing water droplet, Int. J. Heat Mass Tran., 46, 1199–1213, 2003.

Hiranuma, N. and Möhler, O.: Personal communication, 2013.

Hoffer, T. E.: A laboratory investigation of droplet freezing, J. Meteorol., 18, 766–778, 1961.

Hoose, C. and Möhler, O.: Heterogeneous ice nucleation on atmospheric aerosols: a review of results from laboratory experiments, Atmos. Chem. Phys., 12, 9817–9854, doi:10.5194/acp-12-9817-2012, 2012.

Hoose, C., Lohmann, U., Erdin, R., and Tegen, I.: The global influence of dust mineralogical composition on heterogeneous ice nucleation in mixed-phase clouds, Environ. Res. Lett., 3, 025003–025017, 2008.

Kandler, K., Benker, N., Bundke, U., Cuevas, E., Ebert, M., Knippertz, P., Rodríguez, S., Schütz, L., and Weinbruch, S.: Chemical composition and complex refractive index of Saha-

ran mineral dust at Izaña, Tenerife (Spain), derived by electron microscopy, Atmos. Environ., 41, 8058–8074, doi:10.1016/j.atmosenv.2007.06.047, 2007.
Knopf, D. A., Alpert, P. A., Wang, B., and Aller, J. Y.: Simulation of ice nucleation by marine diatoms, Nat. Geosci., 4, 88–90, doi:10.1038/ngeo1037, 2011.
Köster, H. M.: Mineralogical and chemical heterogeneity of three standard clay mineral samples, Clay Miner., 31, 417–422, 1996.
Ladino Moreno, L. A., Stetzer, O., and Lohmann, U.: Contact freezing: a review of experimental studies, Atmos. Chem. Phys., 13, 9745–9769, doi:10.5194/acp-13-9745-2013, 2013.
Leng, Y. and Cummings, P. T.: Hydration structure of water confined between mica surfaces, J. Chem. Phys., 124, 074711, 69–92, 2006.
Lüönd, F., Stetzer, O., Welti, A., and Lohmann, U.: Experimental study on the ice nucleation ability of size selected kaolinite particles in the immersion mode, J. Geophys. Res., 115, D14201, doi:10.1029/2009JD012959, 2010.
Möhler, O., Stetzer, O., Schaefers, S., Linke, C., Schnaiter, M., Tiede, R., Saathoff, H., Krämer, M., Mangold, A., Budz, P., Zink, P., Schreiner, J., Mauersberger, K., Haag, W., Kärcher, B., and Schurath, U.: Experimental investigation of homogeneous freezing of sulphuric acid particles in the aerosol chamber AIDA, Atmos. Chem. Phys., 3, 211–223, doi:10.5194/acp-3-211-2003, 2003.
Murray, B. J., Broadly, S. L., Wilson, T. W., Bull, S., and Wills, R. H.: Kinetics of the homogeneous freezing of water, Phys. Chem. Chem. Phys., 12, 10380–10387, doi:10.1039/C003297B, 2010.
Murray, B. J., Broadley, S. L., Wilson, T. W., Atkinson, J. D., and Wills, R. H.: Heterogeneous freezing of water droplets containing kaolinite particles, Atmos. Chem. Phys., 11, 4191–4207, doi:10.5194/acp-11-4191-2011, 2011.
Niedermeier, D., Hartmann, S., Shaw, R. A., Covert, D., Mentel, T. F., Schneider, J., Poulain, L., Reitz, P., Spindler, C., Clauss, T., Kiselev, A., Hallbauer, E., Wex, H., Mildenberger, K., and Stratmann, F.: Heterogeneous freezing of droplets with immersed mineral dust particles – measurements and parameterization, Atmos. Chem. Phys., 10, 3601–3614, doi:10.5194/acp-10-3601-2010, 2010.
Niemand, M., Möhler, O., Vogel, B., Vogel, H., Hoose, C., Connolly, P., Klein, H., Bingemer, H., Skrotzki, J., and Leisner, T.: A particle-surface-area-based parameterization of immersion freezing on mineral dust particles, J. Atmos. Sci., 69, 3077–3092, doi:10.1175/JAS-D-11-0249.1, 2012.

Phillips, V. T. J., Donner, L. J., and Garner, S. T.: Nucleation processes in deep convection simulated by a cloud-system-resolving model with double-moment bulk microphysics, J. Atmos. Sci., 64, 738–761, 2007.

Pinti, V., Marcolli, C., Zobrist, B., Hoyle, C. R., and Peter, T.: Ice nucleation efficiency of clay minerals in the immersion mode, Atmos. Chem. Phys., 12, 5859–5878, doi:10.5194/acp-12-5859-2012, 2012.

Pitter, R. L. and Pruppacher, H. R.: A wind tunnel investigation of freezing of small water drops falling at terminal velocity in air, Q. J. Roy. Meteor. Soc., 99, 540–550, 1973.

Pruppacher, H. R. and Klett, J. D.: Microphysics of Clouds and Precipitation, 2nd rev. edn., Kluwer Academic Publishers, Dordrecht, 1997.

Pummer, B. G., Bauer, H., Bernardi, J., Bleicher, S., and Grothe, H.: Suspendable macromolecules are responsible for ice nucleation activity of birch and conifer pollen, Atmos. Chem. Phys., 12, 2541–2550, doi:10.5194/acp-12-2541-2012, 2012.

Storelvmo, T., Kristjánsson, J. E., and Lohmann, U.: Aerosol influence on mixed-phase clouds in CAM-Oslo, J. Atmos. Sci., 65, 3214–3230, 2008.

Vali, G.: Repeatability and randomness in heterogeneous freezing nucleation, Atmos. Chem. Phys., 8, 5017–5031, doi:10.5194/acp-8-5017-2008, 2008.

v. Blohn, N., Mitra, S. K., Diehl, K., and Borrmann, S: The ice nucleating ability of pollen, Part III: New laboratory studies in immersion and contact freezing modes including more pollen types, Atmos. Res., 78, 182–189, 2005.

Zuberi, B., Bertram, A. K., Cassa, C. A., Molina, L. T., and Molina, M. J.: Heterogeneous nucleation of ice in $(NH_4)2SO_4$-H_2O particles with mineral dust immersions, Geophys. Res. Lett., 29, 1504, doi:10.1029/2001GL014289, 2002.

Table 1. Experimental conditions during freezing experiments.

particle type	specific surface area $m^2\,g^{-1}$	drop radius mm	particle surface area $m^2\,drop^{-1}$	median freezing temperature °C
montmorillonite K10	220	1 ± 0.05	$(2.5 \pm 0.1) \times 10^{-4}$	-20.6 ± 0.7
illite IMt1	31.7	1 ± 0.05	$(3.5 \pm 0.2) \times 10^{-6}$	-23.6 ± 0.7
		1 ± 0.05	$(3.5 \pm 0.2) \times 10^{-5}$	-22.1 ± 0.7
		1 ± 0.05	$(7.0 \pm 0.4) \times 10^{-5}$	-18.8 ± 0.7
illite NX	124.4	1 ± 0.05	$(7.1 \pm 0.3) \times 10^{-7}$	-23.7 ± 0.7
		1 ± 0.05	$(7.1 \pm 0.3) \times 10^{-6}$	-22.8 ± 0.7
		1 ± 0.05	$(7.1 \pm 0.3) \times 10^{-5}$	-19.7 ± 0.7
		0.34 ± 0.03	$(5.1 \pm 1.3) \times 10^{-6}$	-20.8 ± 1.0
		0.34 ± 0.03	$(5.1 \pm 1.3) \times 10^{-5}$	-19.2 ± 1.0

ACPD
14, 12887–12930, 2014

Particle-area dependence of mineral dust in the immersion mode

K. Diehl et al.

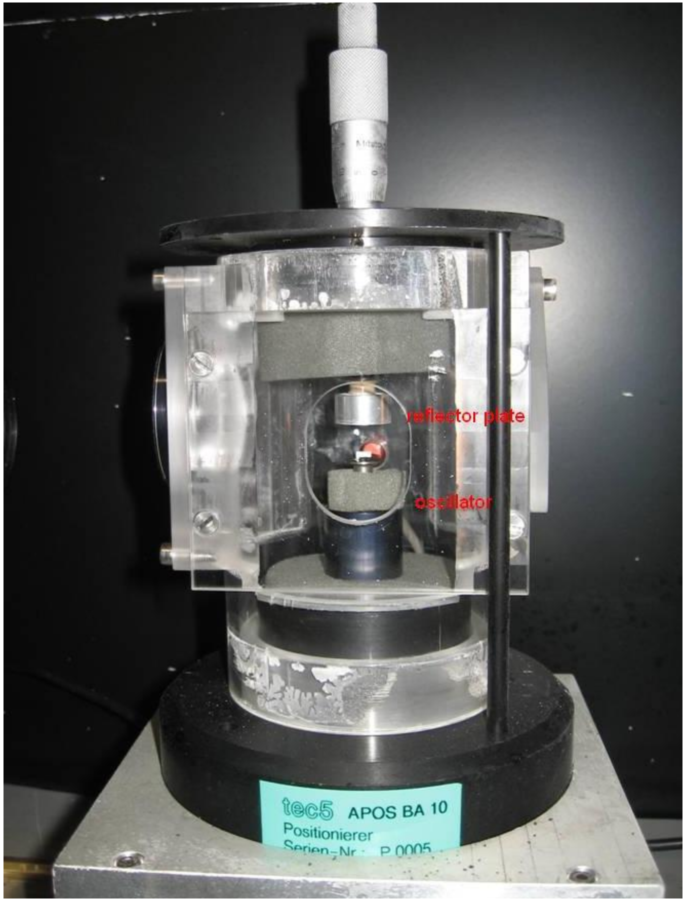

Figure 1. Acoustic levitator.

ACPD
14, 12887–12930, 2014

Particle-area dependence of mineral dust in the immersion mode

K. Diehl et al.

Title Page
Abstract Introduction
Conclusions References
Tables Figures
◂ ▸
Back Close
Full Screen / Esc
Printer-friendly Version
Interactive Discussion

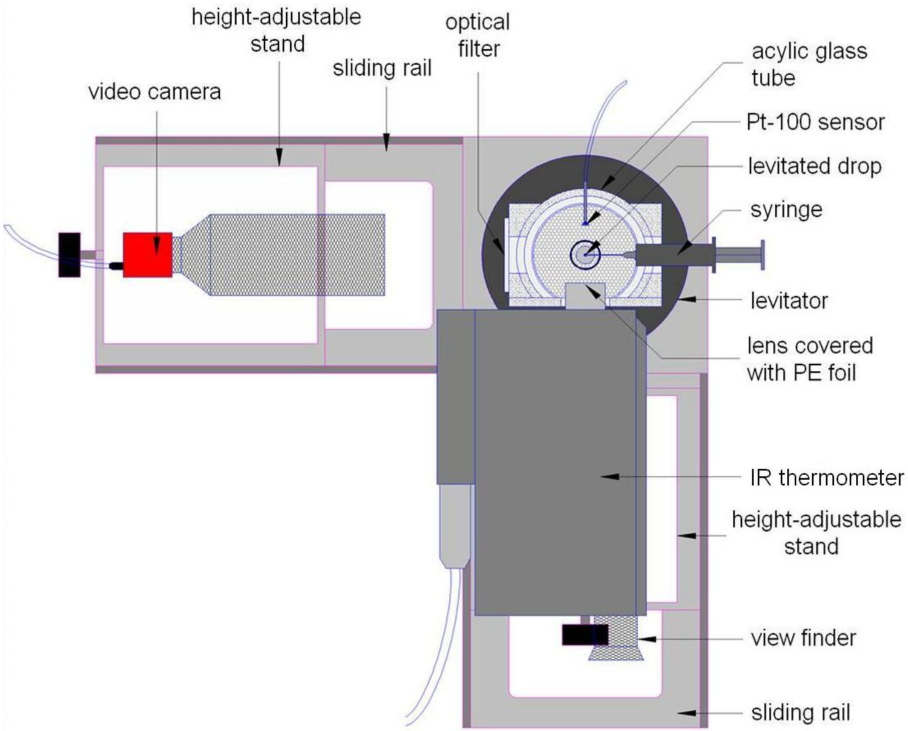

Figure 2. Scheme of the experimental setup with the acoustic trap in the cold chamber.

ACPD
14, 12887–12930, 2014

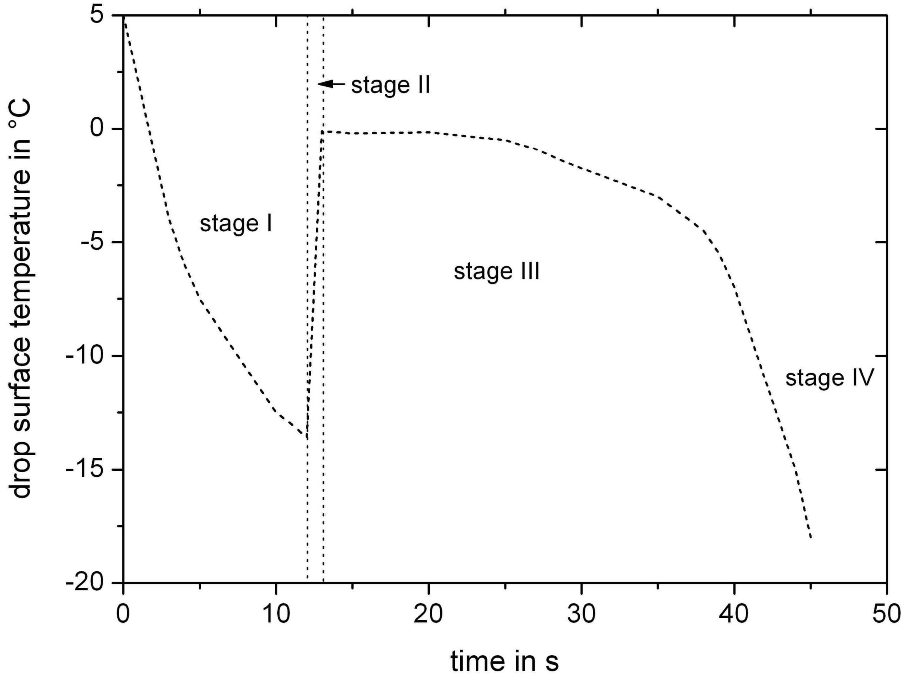

Figure 3. Example of the development of the drop temperature with time during freezing.

ACPD
14, 12887–12930, 2014

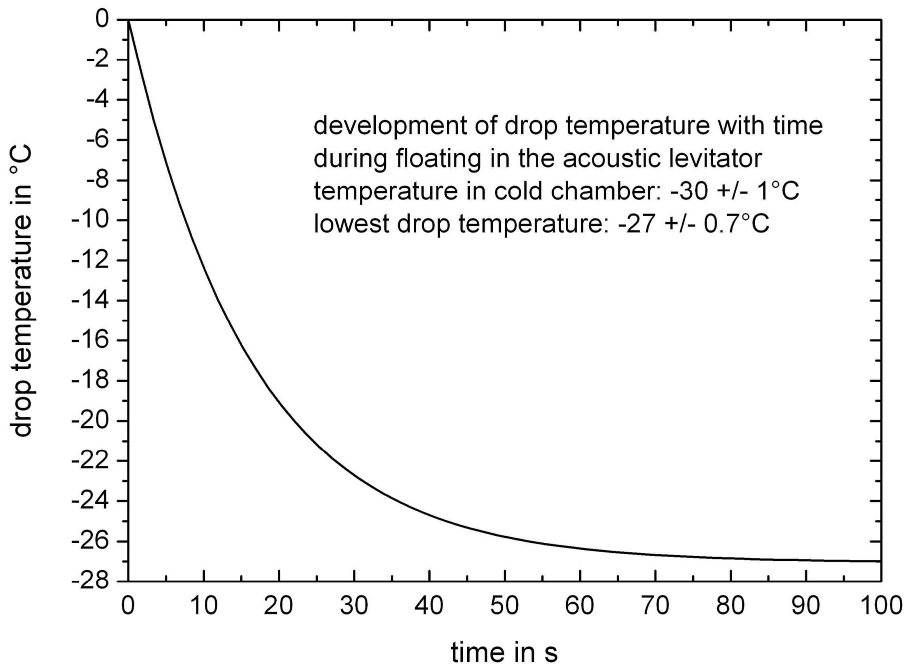

Figure 4. Development of drop temperature during freely floating in the acoustic levitator at a cold chamber ambient temperature of −30 °C.

ACPD
14, 12887–12930, 2014

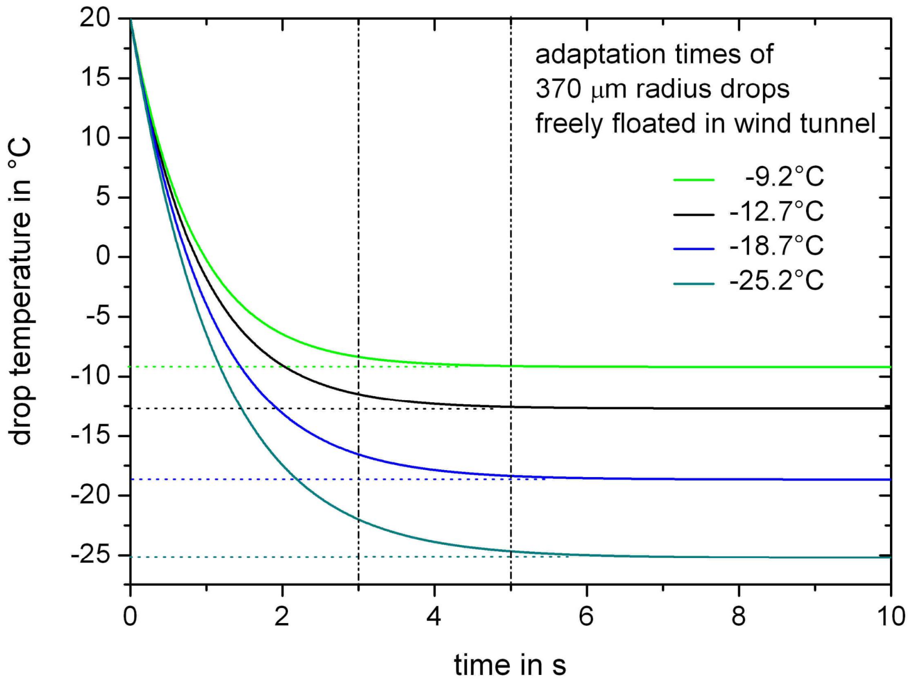

Figure 5. Calculated adaptation times of 370 radius drops while freely floating in the wind tunnel at various ambient temperatures.

ACPD
14, 12887–12930, 2014

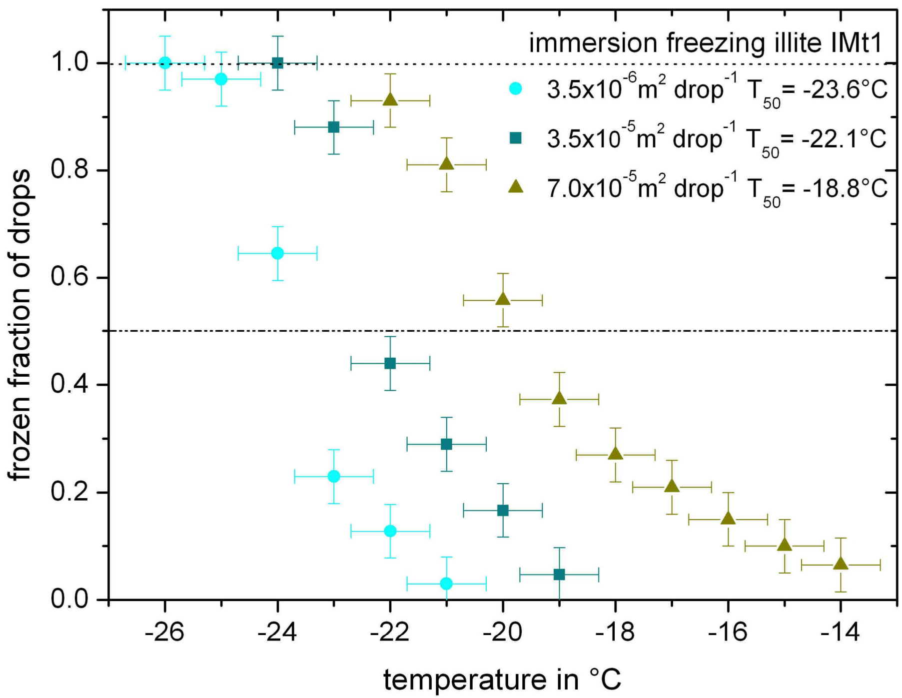

Figure 6. Immersion freezing of illite IMt1 in the acoustic levitator: frozen fraction of drops as function of temperature for three different particle surface areas per drop.

ACPD
14, 12887–12930, 2014

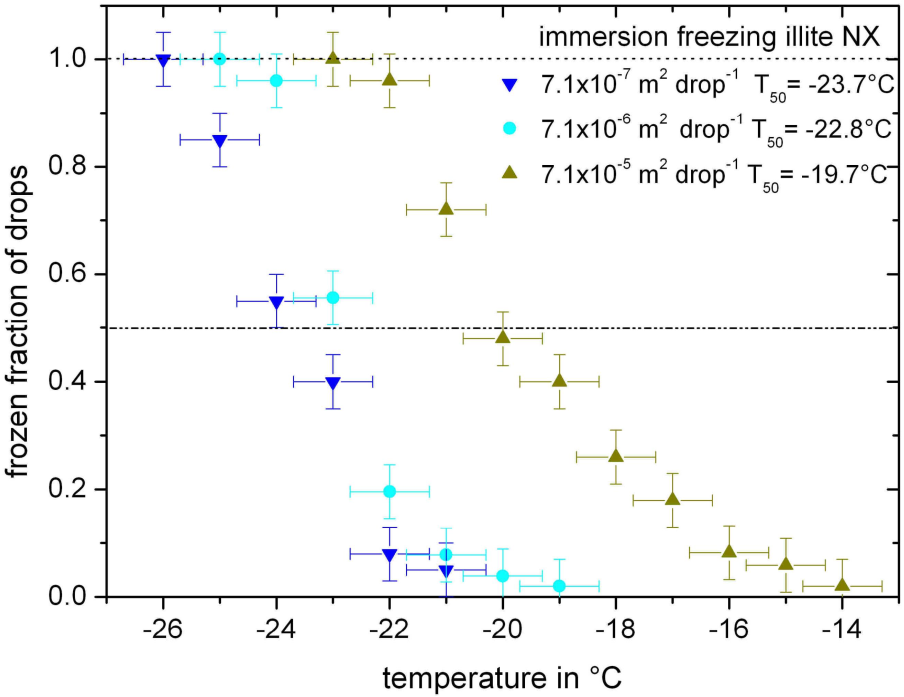

Figure 7. Immersion freezing of illite NX in the acoustic levitator: frozen fraction of drops as function of temperature for three different particle surface areas per drop.

ACPD
14, 12887–12930, 2014

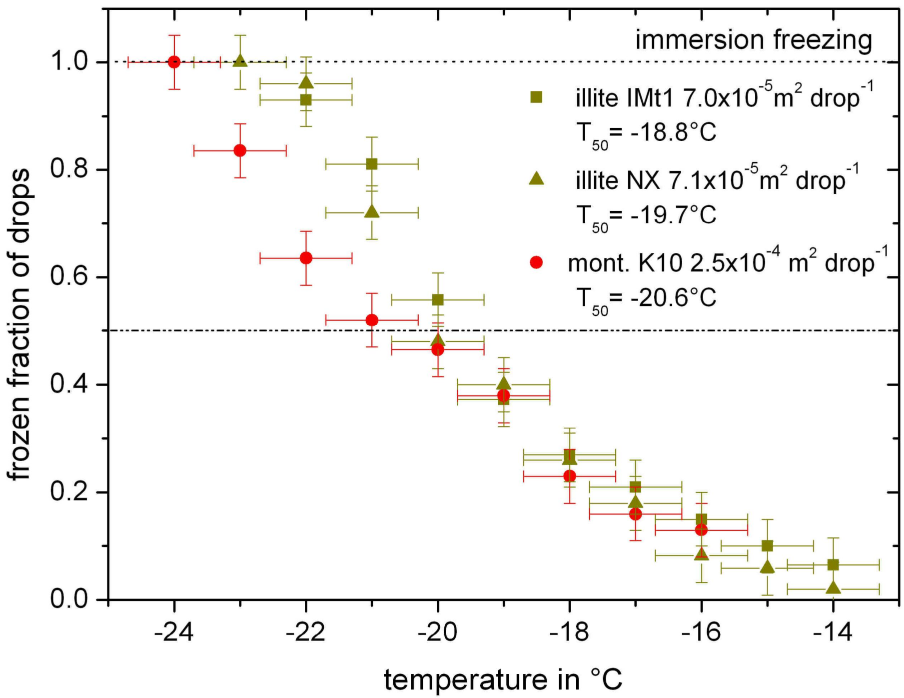

Figure 8. Immersion freezing for montmorillonite K10 in comparison to illite: frozen fraction of drops as function of temperature.

ACPD
14, 12887–12930, 2014

Title Page
Abstract Introduction
Conclusions References
Tables Figures
◀◀ ▶▶
◀ ▶
Back Close
Full Screen / Esc
Printer-friendly Version
Interactive Discussion

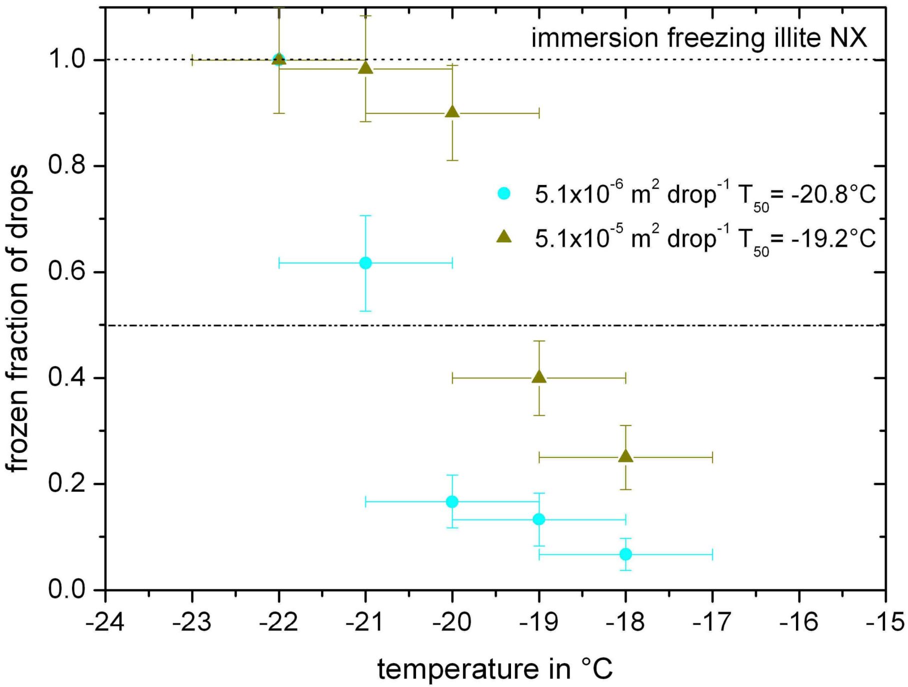

Figure 9. Immersion freezing of illite NX in the wind tunnel: frozen fraction of drops as function of temperature for two different particle surface areas per drop. Accumulated values within total observation time of 30 s.

ACPD
14, 12887–12930, 2014

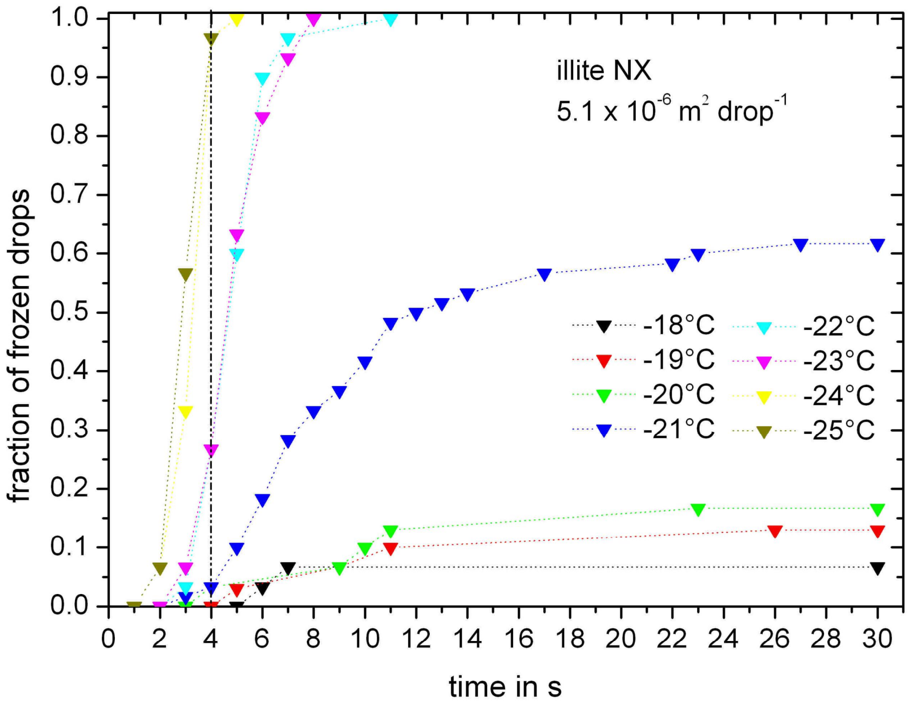

Figure 10. Time resolved frozen fractions measured in the wind tunnel with illite NX present with 5.1×10^{-6} m^2 per drop at different temperatures.

ACPD
14, 12887–12930, 2014

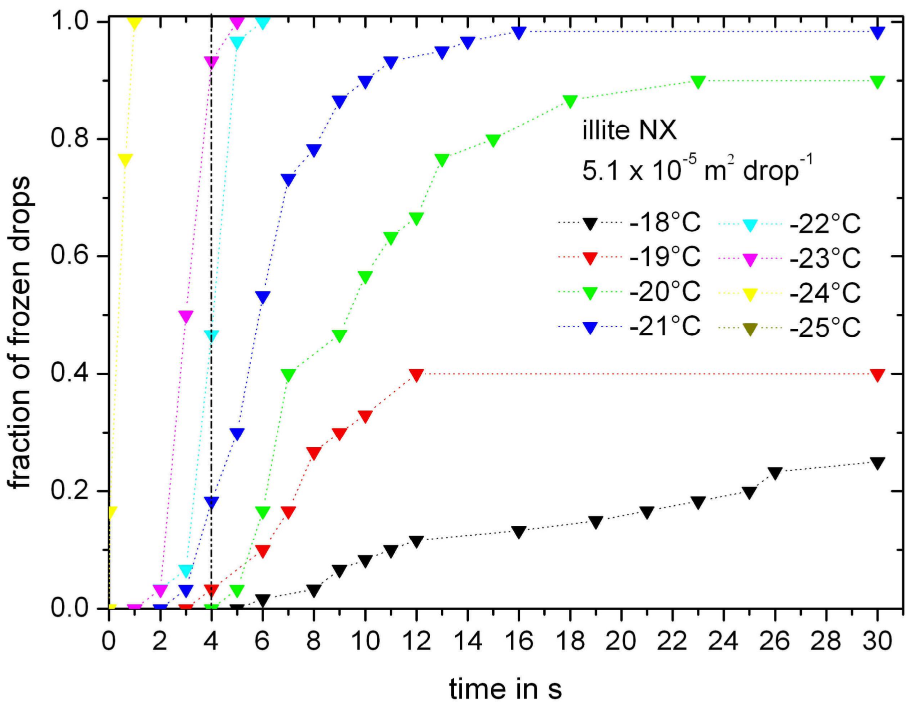

Figure 11. Time resolved frozen fractions measured in the wind tunnel with illite NX present with 5.1×10^{-5} m^2 per drop at different temperatures.

ACPD
14, 12887–12930, 2014

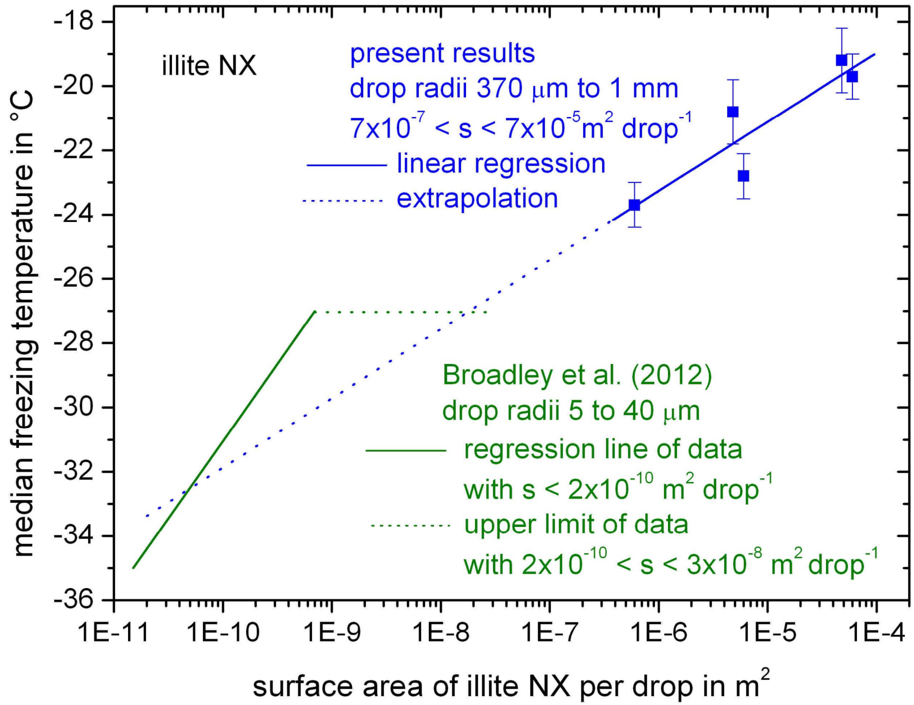

Figure 12. Median freezing temperatures of illite for various surface areas per drop. Solid blue line with symbols: present experiments from acoustic levitator and wind tunnel, dotted blue line: extrapolation. Green: results from Broadley et al. (2012).

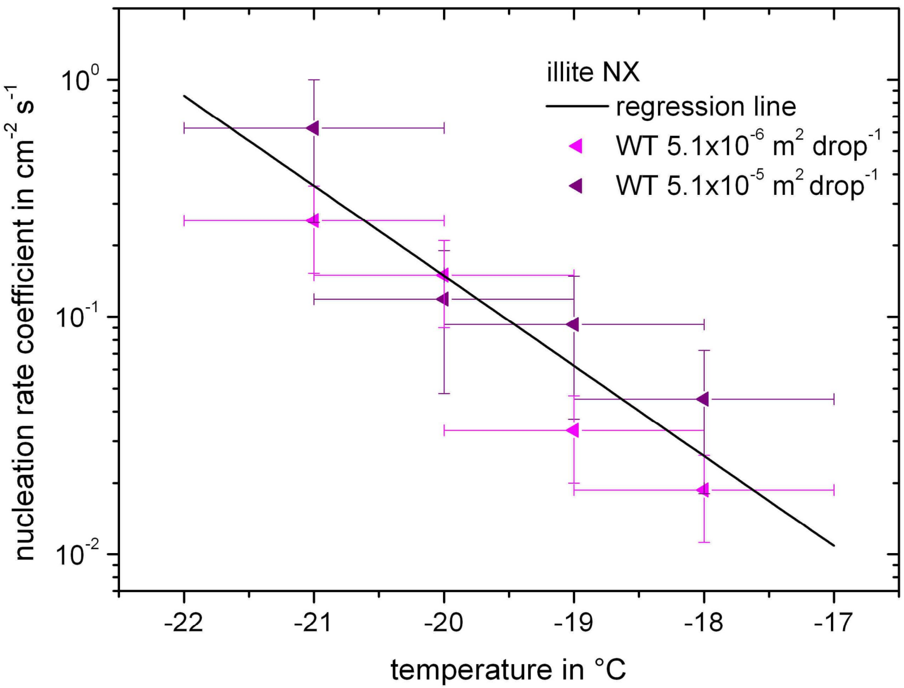

Figure 13. Nucleation rate coefficients as function of temperature for illite NX for two particle surface areas per drop, investigated in the wind tunnel.

ACPD
14, 12887–12930, 2014

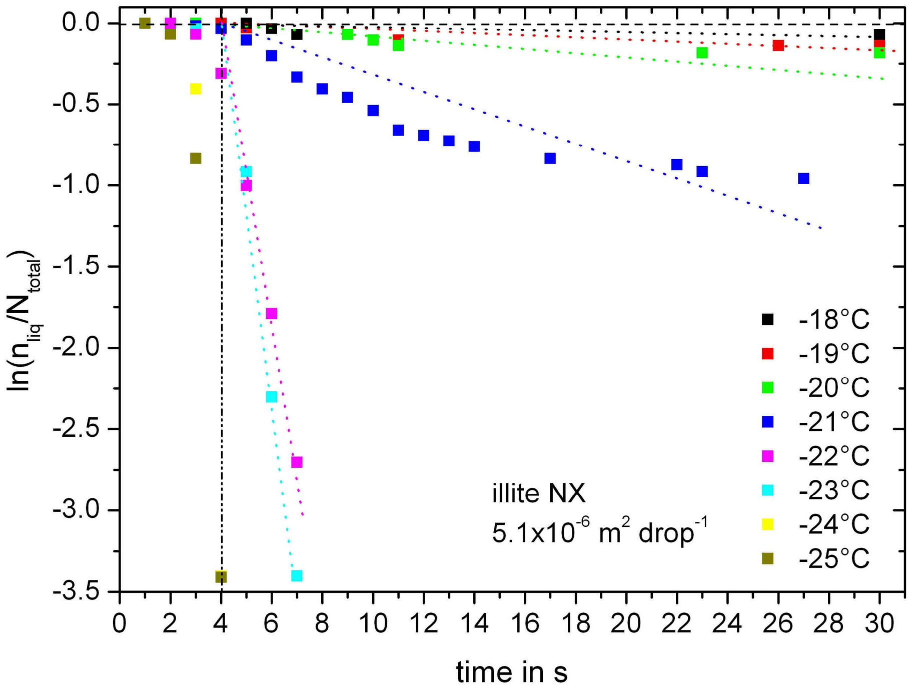

Figure 14. Liquid ratio as function of time from wind tunnel experiments at different temperatures, illite NX present with 5.1×10^{-6} m^2 per drop. Vertical line: limit of adaptation time of the drops.

ACPD
14, 12887–12930, 2014

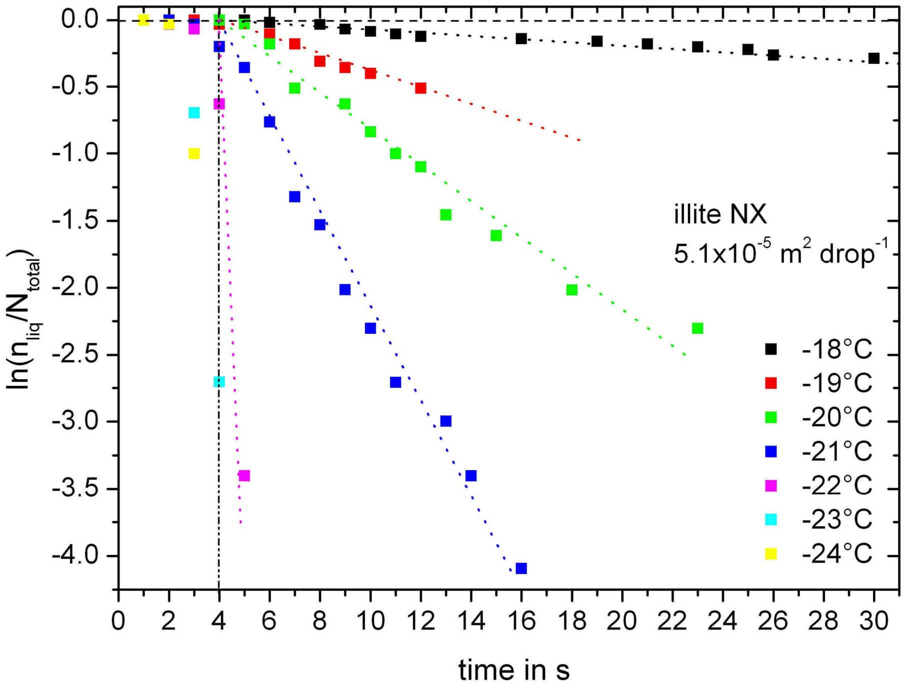

Figure 15. Liquid ratio as function of time from wind tunnel experiments at different temperatures, illite NX present with 5.1×10^{-5} m^2 per drop. Vertical line: limit of adaptation time of the drops.

ACPD
14, 12887–12930, 2014

Particle-area dependence of mineral dust in the immersion mode

K. Diehl et al.

Title Page
Abstract | Introduction
Conclusions | References
Tables | Figures
◀| |▶
◀ ▶
Back | Close
Full Screen / Esc
Printer-friendly Version
Interactive Discussion

ACPD
14, 12887–12930, 2014

Particle-area dependence of mineral dust in the immersion mode

K. Diehl et al.

Title Page
Abstract | Introduction
Conclusions | References
Tables | Figures
◀| |▶
◀ ▶
Back | Close
Full Screen / Esc
Printer-friendly Version
Interactive Discussion

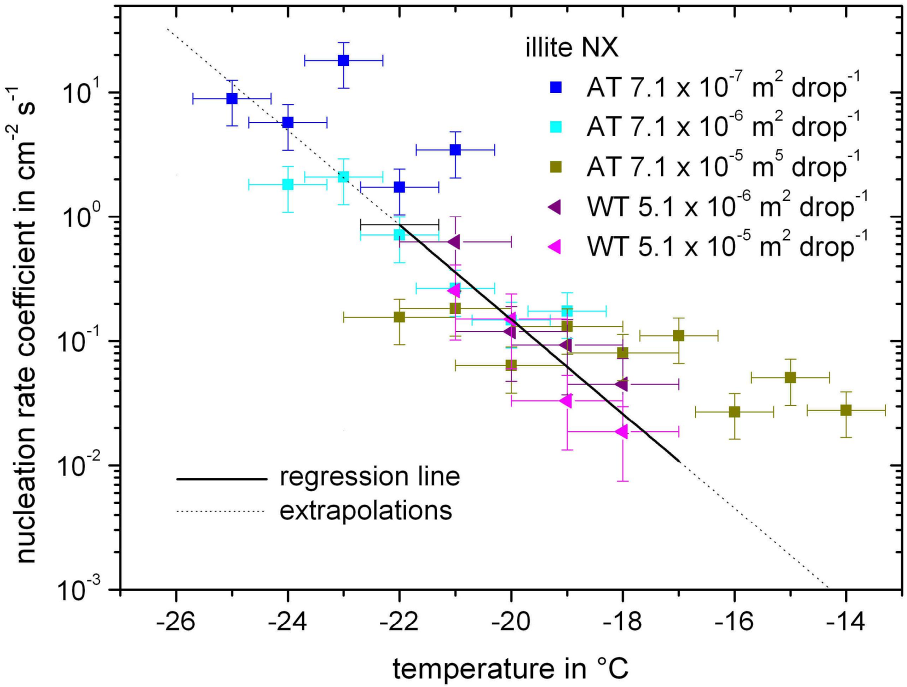

Figure 16. Nucleation rate coefficients as function of temperature for illite NX for various particle surface areas per drop, determined by two experimental techniques.

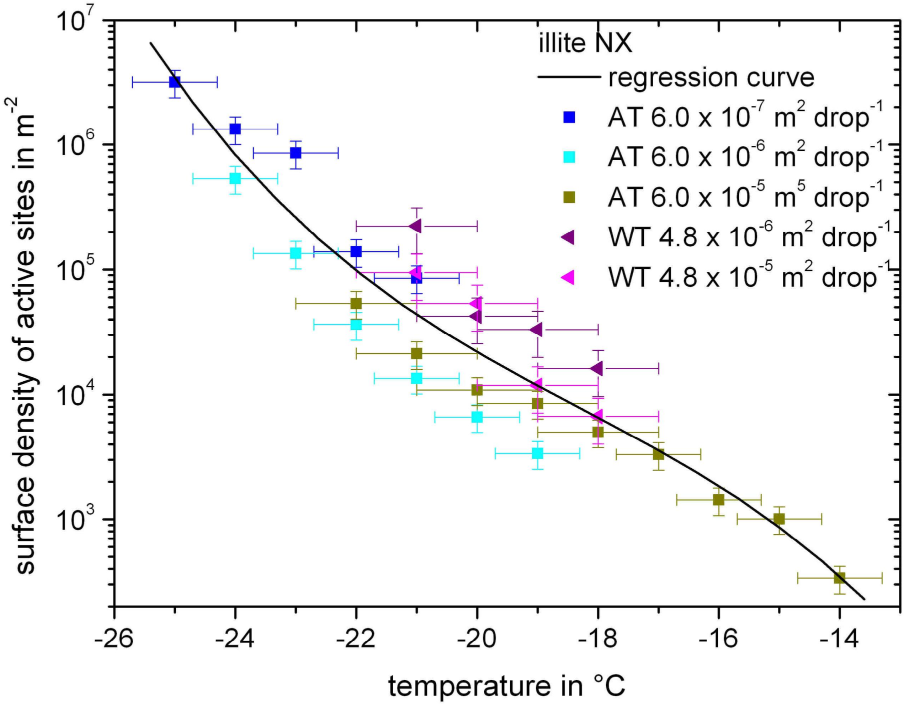

Figure 17. Surface density of illite NX as function of temperature for various particle surface areas per drop, determined by two experimental techniques.

ACPD
14, 12887–12930, 2014

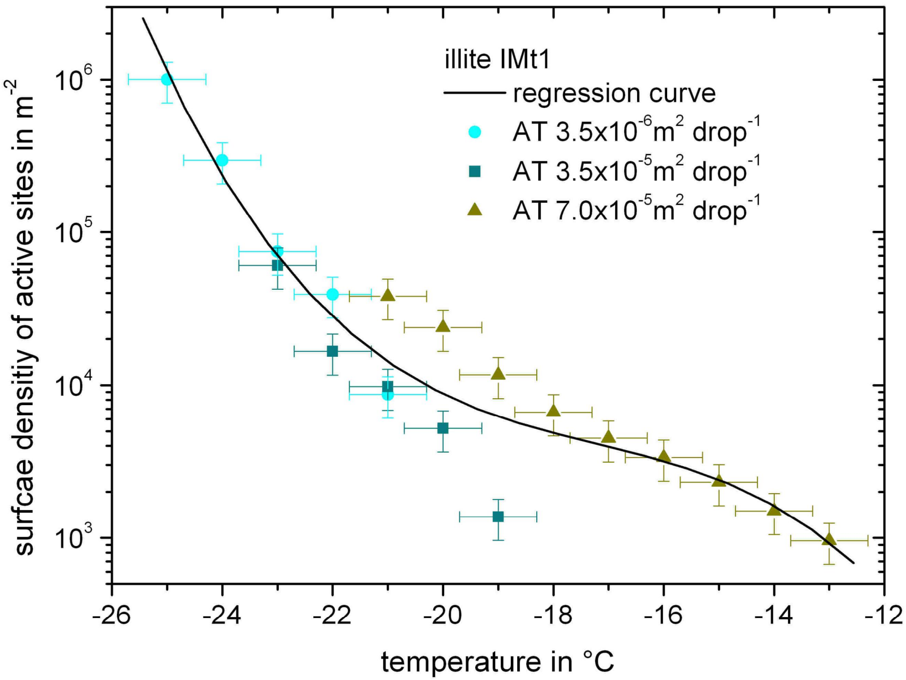

Figure 18. Surface density of illite IMt1 as function of temperature for various particle surface areas per drop, determined by the acoustic levitator.

ACPD
14, 12887–12930, 2014

Particle-area dependence of mineral dust in the immersion mode

K. Diehl et al.

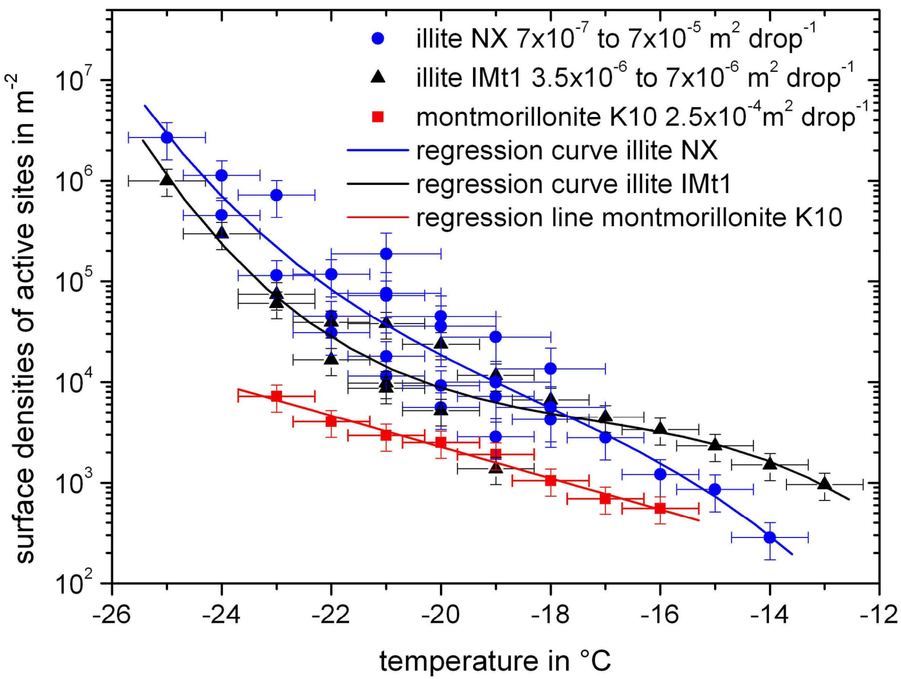

Figure 19. Comparison of the surface densities of illite NX and IMt1.

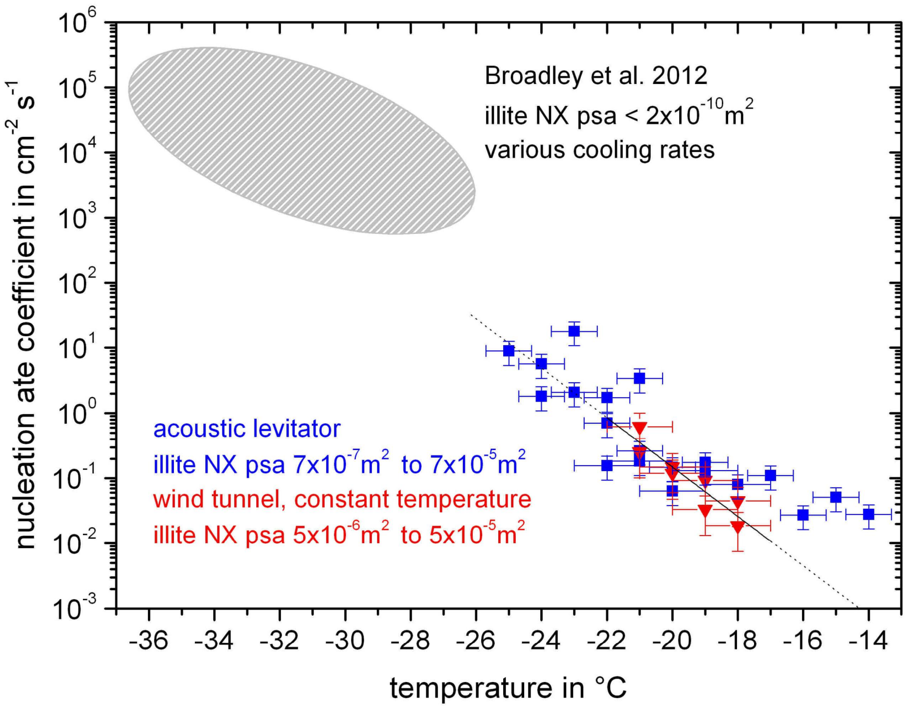

Figure 20. Nucleation rate coefficients for illite NX derived from present (shown in blue and red) and previous experiments (indicated as grey region, from Broadley et al., 2012).

ACPD
14, 12887–12930, 2014

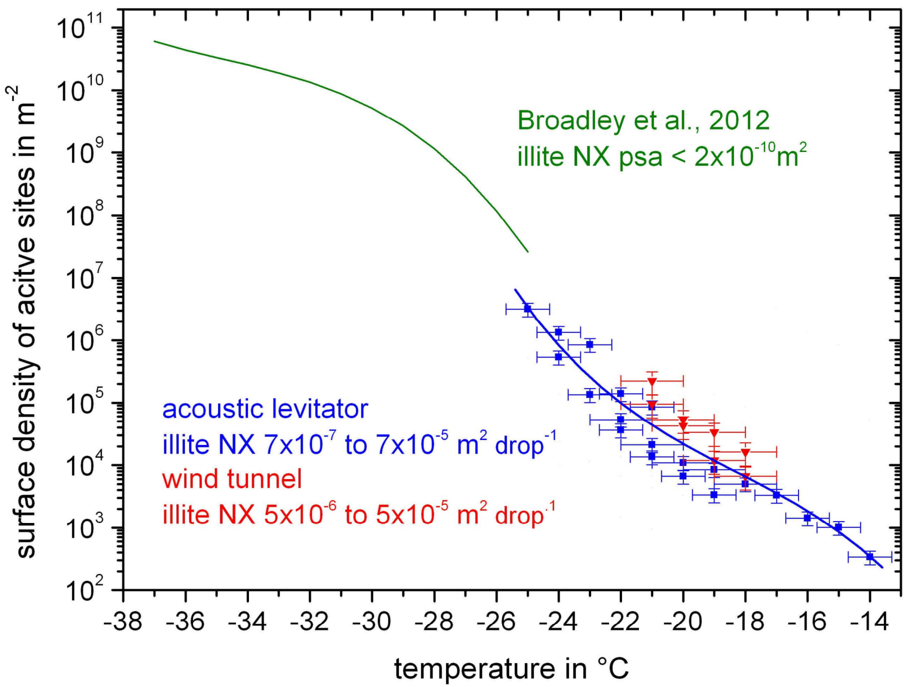

Figure 21. Surface densities of active sites for illite NX derived from present (shown in blue and red) and previous experiments (shown in green, from Broadley et al., 2012).

ACPD
14, 12887–12930, 2014

Particle-area dependence of mineral dust in the immersion mode

K. Diehl et al.